Experimental Research on the Nanoindentation of Bovine Compact Bone under Fatigue Loading

Xianjia Meng
Tianjin University
Qinghua Qin
Australian National University
Chuanyong Qu (qu_chuanyong@tju.edu.cn)
Tianjin University https://orcid.org/0000-0002-7249-9440

Research

Keywords: Bone fatigue damage, Creep, Micromechanics, Fatigue test methods, Nanoindentation

Posted Date: January 25th, 2021

DOI: https://doi.org/10.21203/rs.3.rs-153151/v1

Experimental Research on the Nanoindentation of Bovine Compact Bone under Fatigue Loading

Xianjia Meng [1], Qinghua Qin[2] and Chuanyong Qu [1,*]

*Correspondence: qu_chuanyong@tju.edu.cn

[1] Department of Mechanics, School of Mechanical Engineering, Tianjin University, Tianjin 300350, China

[2] College of Engineering and Computer Science, Australian National University, Canberra, ACT 2601, Australia

Abstract

Background: The role of bone fatigue damage at the nanostructural level, and its effect on fatigue properties is an understudied and important subject. An understanding of the subtler aspects of bone's properties is crucial to understanding bone fragility caused by aging, disease, and fatigue damage. The primary strength of this study was the demonstration of the degradation of bone's microscopic mechanical properties by nanoindentation following fatigue loading.

Methods: Nanoindentation was used to probe the micro-mechanical properties of bovine tibiae subjected to fatigue loading in four-point bending. Indentation tests were conducted in the same 30×120 μm region before fatigue loading and after loading to fracture. We analysed the effects of residual indentations on bone's fatigue resistance using an optical microscope and scanning electron microscope. The mechanical properties calculated using nanoindentation were reduced modulus and hardness, the time constant based on creep, long-term creep viscosity and the dissipated work. Differences of each parameter before loading and post fracture were examined using paired t-tests.

Results: The morphology of the initial residual indentation before fatigue loading appeared the same as that after loading to fracture. The results show that the reduced modulus decreased significantly ($p=9.47\times10^{-3}$) by 7.62%~15.16% after fracture whereas the time constant of creep increased slightly ($p=0.049$) by 2.81%~5.41%. The p-value was significantly lower ($p<0.001$) for reduced modulus compared to all other mechanical properties.

Conclusion: Residual indents different from fatigue damage created no crack initiators that would weaken bone's resistance to fatigue loading. Fatigue loading has the most heavy effect on bone's reduced modulus compared to all other microscopic mechanical properties.

Keywords: Bone fatigue damage; Creep; Micromechanics; Fatigue test methods; Nanoindentation

1. Introduction

Bone is a natural composite material with a multiscale structure[1-4]. Bone's strength and damage resistance result from its nanocomposite properties [5, 6]. Micro-mechanical property degradation in bone tissue with fatigue is a crucial component of the ability to understand and predict damage-related fracture [7-9]. It is well-known that fatigue damage is present at the nanoscale, characterized by molecular uncoiling and fibrillar sliding with much smaller scale than linear cracks and diffuse damage [10-12]. So, bone's micromechanical properties under fatigue loading need to be determined for a better understanding of damage mechanisms.

Nanoindentation [13, 14] is an increasingly frequently used technique for the mechanical characterization of bone's microstructure [15-18]. This method has shown good results in the modeling of damage laws [19, 20], avoiding confounding factors such as microcracks and porosity that affect bone's macroscopic properties [21, 22]. As the required test area for nanoindentation is at the microscopic level [23, 24], the mechanical properties after fracture can still be captured. The viscoelastic properties of bone also can be calculated from the displacement-time curves[25-27]. Bone exhibits both creep and stress relaxation but the viscoelasticity of collagen fibers may affect bone fragility [28-30]. Time-dependent viscoelastic properties before fatigue and after fracture should be determined. Moreover, in addition to demands of studies on alterations in bone architecture (e.g., diffuse damage, linear microcracks, etc.), the investigation of mechanical properties of the remaining bone components (where inelastic deformation and microfracture may occur at any time) also is important [8, 9]. Studies of the interaction of fatigue damage with bone micromechanical properties will provide better understanding of bone fracture[31]. Further, the post-fracture mechanical properties of bone have been largely neglected in macroscopic experiments due to technical difficulties in conducting such tests [32-34]. The fatigue induced deterioration of micro-mechanical properties that cannot be captured by bulk measurements can be

determined using nanoindentation. However, micromechanical properties following fatigue damage determined using nanoindentation are characterized incompletely in cortical bone.

The aim of this study was to investigate bone's micro-mechanical properties under fatigue loading. Nanoindentation tests were conducted in the loaded area before fatigue and after fracture. Due to the assumptions of this method and the complex structure of bone, values reflect relative mechanical properties at the microscopic scale and allow these relative differences to be compared to provide a more complete picture of damage-related fatigue processes.

2. Materials and Methods

2.1. Specimen preparation

Five tibia from 24 month old cattle were collected from the slaughterhouse and dehydrated. Five specimens cut from the postero-lateral aspect of the cortex were polished into rectangular cubes with coarse sandpaper [35-37]. Fine sandpaper was used to refine the surface to meet the requirements for nanoindentation. The final specimens were 5.0±0.15 mm × 5.0±0.15 mm × 30±0.15 mm. The bone was kept cooling with buffered saline throughout the cutting and polishing process[38, 39]. No obvious pathology or cracks (larger than 100 um) were observed on the surface of the bone specimens by light microscope. The root mean square surface roughness in the initial unfatigued and post-fracture period were both less than 60 nm on a 20×20 um AFM scan (FM-Nanoview1000AFM, Frequency: 50Hz/60Hz) [40]. The surfaces of the specimens were not only parallel to each other but also parallel to the longitudinal direction. The angle between each pair of planes was 90◦, with a maximum deviation of 2.5%. In addition, four silica reference samples were prepared. Two of them had perfectly smooth surfaces and the others were polished using the same protocol for the bone samples.

2.2. Fatigue test

The contact points in three-point bending tests make it difficult to separate the damage caused by fatigue from the stress concentration created by the loading point. Thus, four-point bending(Figure 1) was used in this study with a sinusoidal wave and a frequency of 10 Hz so that the region between the inner contacts was under pure bending[41]. The inner span (b) was 10mm and the outer span (b+2a) was 20mm. Load-controlled fatigue loading was performed using an Electro-Puls-Instron(E10000N, USA) with a range of 10kN and a accuracy of 0.001N. The sample had a thickness of d, width of w and $F=\sigma_{max}\cdot wd^2/3a$. The maximum stress σ_{max} used in this study

was 100 MPa and the average stress σ_m was 45 MPa. The contact radius was 2.0mm. This is sufficient to avoid stress concentration. Each specimen was fatigue loaded to failure (Table 1).

2.3. Nanoindentation test

The initial indentation test was conducted before loading while the second test was conducted after loading to fracture. All bone specimens were oriented similarly and indented in the longitudinal direction. The Hysitro TI-Premier (produced by the American Hysitron Inc company) was used to perform the nanoindentation tests. A load-controlled indentation protocol was used. The tip was loaded into the sample at a rate of 2 mN/s, held at a maximum load of 10 mN for 10 s, and then unloaded at a rate of 2 mN/s, resulting in ~1600 nm deep indentations. The hardness H and the reduced modulus E_r were calculated using the Oliver and Pharr method from the unloading curves [13]:

$$\frac{1}{E_r} = \frac{1-\nu_{sample}^2}{E_{sample}} + \frac{1-\nu_{indentation}^2}{E_{indentation}}$$

$$E_r = \frac{S\sqrt{\pi}}{2\sqrt{A}}$$

Where υ is Poisson's ratio, $E_{indentation}$=1140GPa, and $\upsilon_{indentation}$=0.07. The hardness H is calculated by

$$H = \frac{P_{\max}}{A}$$

The microstructure of the bone was described using an optical microscope for each indent site. All indents were in the interstitial lamellar bone, that is the highly organized matrix away from osteons and pores. The test area for nanoindentation was 30×120 μm in this study. Each sample was indented six times on the compressive surface of the bone specimens. The space between each indentation was 20μm, 12 times greater than the indentation depth. The indentation sites for two tests were located within 30 um. This chosen area also validated the comparability of each test. Selection of indentation location and the detailed experimental process are shown in Figure 1.

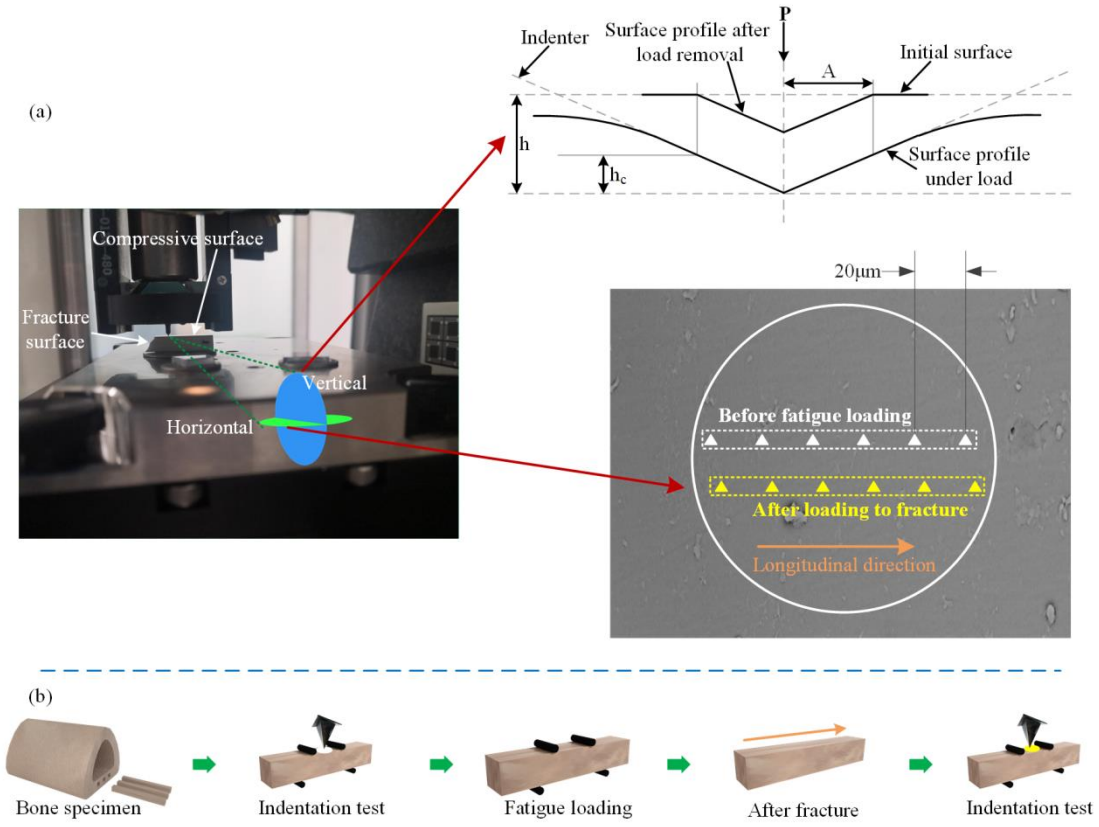

Fig. 1 - A graphic of the indentation test. (a) Bone samples were affixed to the measuring gasket using double-sided adhesive tape. (b) According to the Oliver and Pharr method, the area of contact at peak load is determined by the geometry of the indenter and the depth of contact, $A=F(h_c)$. (c) To avoid mutual influence between indentations, the spacing of each indentation should be at least 5 times greater than the indentation depth. The setting in this study (more than 12 times) meets this requirement.

2.4. Creep

The thermal drift of the indenter was about ±0.1–0.2 nm/s[27]. The average creep rate of all the indentations was greater than 10 nm/s, which is sufficient to minimize the effect of thermal drift [27]. As shown in figure 2, a Burgers model was used in this study.

$$h^2(t)=\frac{\pi}{2}P_0\cot\alpha(1-\nu^2)[\frac{1}{E_1}+\frac{1}{E_2}(1-e^{-t/\tau})+\frac{1}{\eta(1-\nu^2)}t]$$

where P_0 is the peak force (10mN for this study), α is the equivalent cone semi-angle (35.26° for a cube corner indenter), η is the long-term creep viscosity (GPas) and τ is the creep time constant (s). η and τ were determined by minimizing the mean square error between the time–deformation

curve and the equation above using the Nelder–Meadsimplex method (Matlab R2014a, Mathworks Inc., USA).

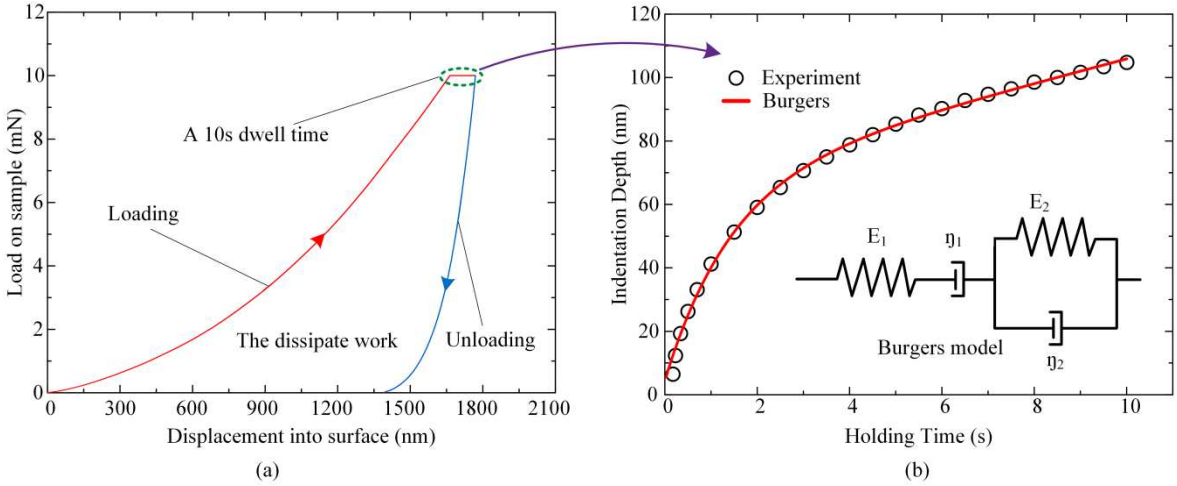

Fig. 2 - A graphic of the load-displacement curves and creep data. (a) The area bound by the load-displacement curve is dissipated work. (b) A representative creep data set and curve fits for the Burgers model with two elastic and two viscous elements. The time constant is theoretically given by E_2/η_2.

2.5.Dissipated work

The dissipated work for each indentation was calculated by integrating the area bound by the load-displacement curve[42]. As shown in Figure 2, the area between the red loading and the blue unloading curves reflects the plastic deformation if the unloading data are assumed to be mostly elastic. This area is called “dissipated work” for irreversible deformation and is used to study the evolution of energy with fatigue loading.

2.6. Statistical analysis

Statistical analysis was performed with SPSS (IBM SPSS Statistics 26). The coefficient of variation (CV%) was calculated for bone specimens and the reference materials. The value of each indentation measurement was used in all statistical analyses. Differences of results before loading and after loading to fracture were examined using paired t-tests (p-value) after pooling the repeated measurements for each parameter. The results of all parameters were expressed as mean and standard deviation (SD). The significance (P_a) of every parameter was calculated as follows:

$$p_a = \frac{1}{n}\sum_{i=1}^{n} p_i$$

Where p_i represents the p-value of each sample before fatigue loading and after loading to fracture, n=5.

3. Results

3.1. Optical microscope and Scanning Electron Microscope (SEM) images of the residual indentations

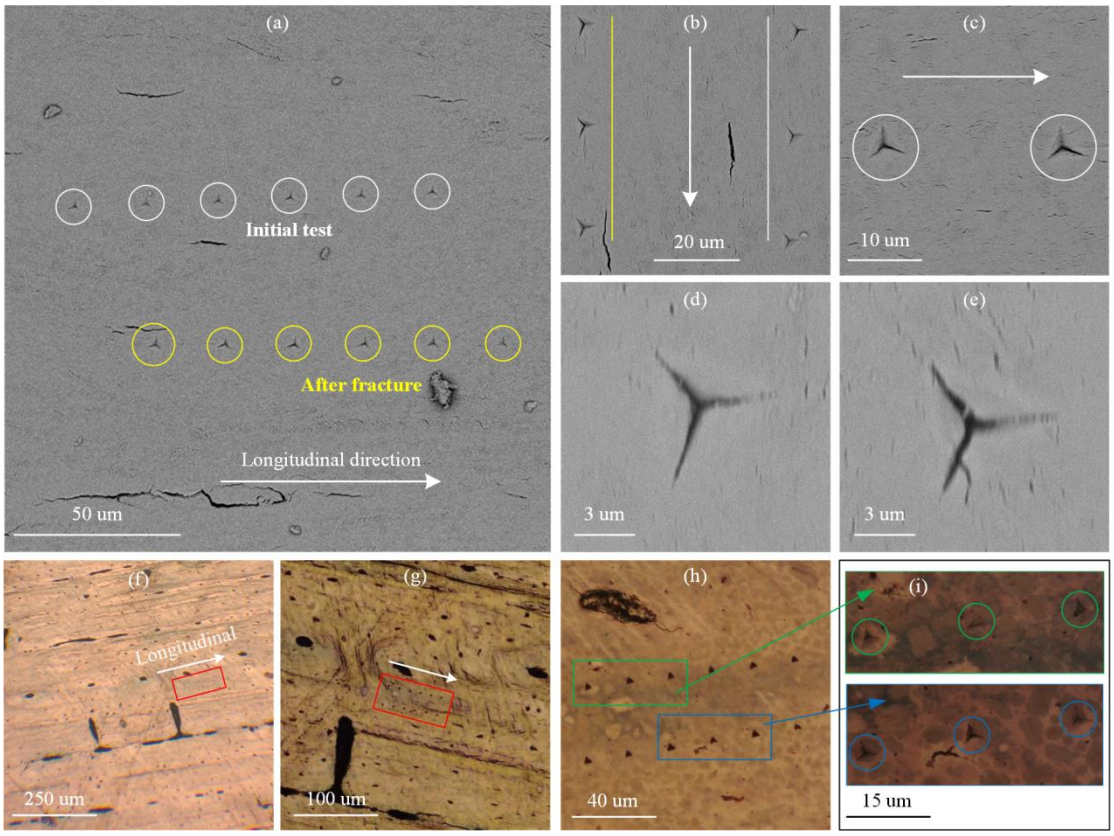

Fig. 3 - A graphic of the residual indentations. (a) & (b) the residual indentations before fatigue loading and after loading to fracture. (c), (d) & (e) the residual indentation morphology left by the initial test after loading to fracture. (f) (g) (h) (i) Optical microscope images. The red is the residual indentations from the two tests. The green is the initial test and the blue is the second test.

The initial test was conducted before fatigue while the second on was done after fracture. As shown in Figure 3, the indentations from the first test still remained a clear original shape after loading to fracture. The residual indentations from two tests were almost the same morphologically. The fracture surface (Fig.1a), where the main failure crack originated from, was several millimeters

away from the indentations site. Residual indents different from fatigue damage created no larger crack initiators that would weaken bone's resistance to fatigue loading.

3.2. Reduced modulus

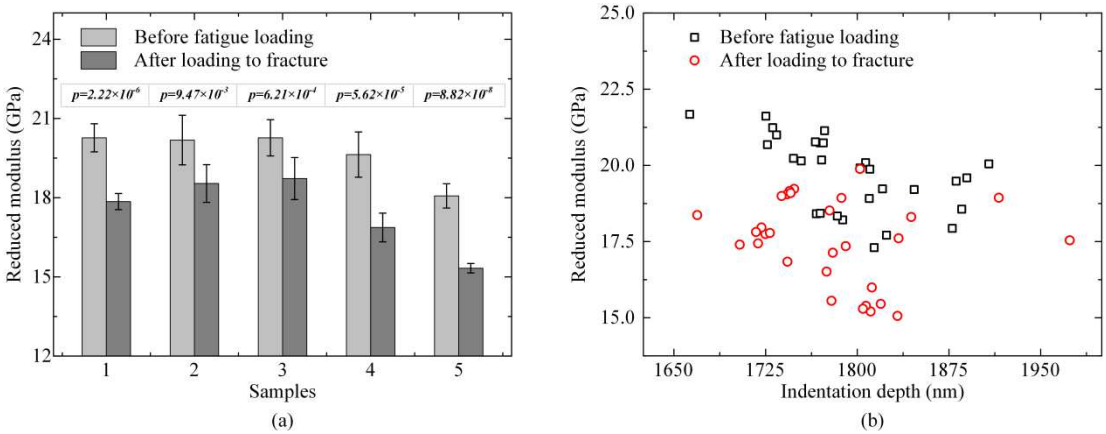

Fig. 4 - A graph of the reduced modulus. (a) The reduced modulus of each sample. (b) The reduced modulus of all samples.

Before fatigue, the averaged reduced modulus was 19.75±1.16 GPa. After fracture the reduced modulus changed to 17.49±1.39 GPa. The averaged modulus decreased by 11.5% during the whole fatigue process. Each sample's reduced modulus decreased obviously which was 7.62% at least and 15.16% at most. The p-value for reduced modulus was less than 0.001 in each sample. There was no obvious variation of the distribution of modulus with the depth before fatigue loading and after loading to fracture (Fig. 4b).

3.3. Creep (Figure 5)

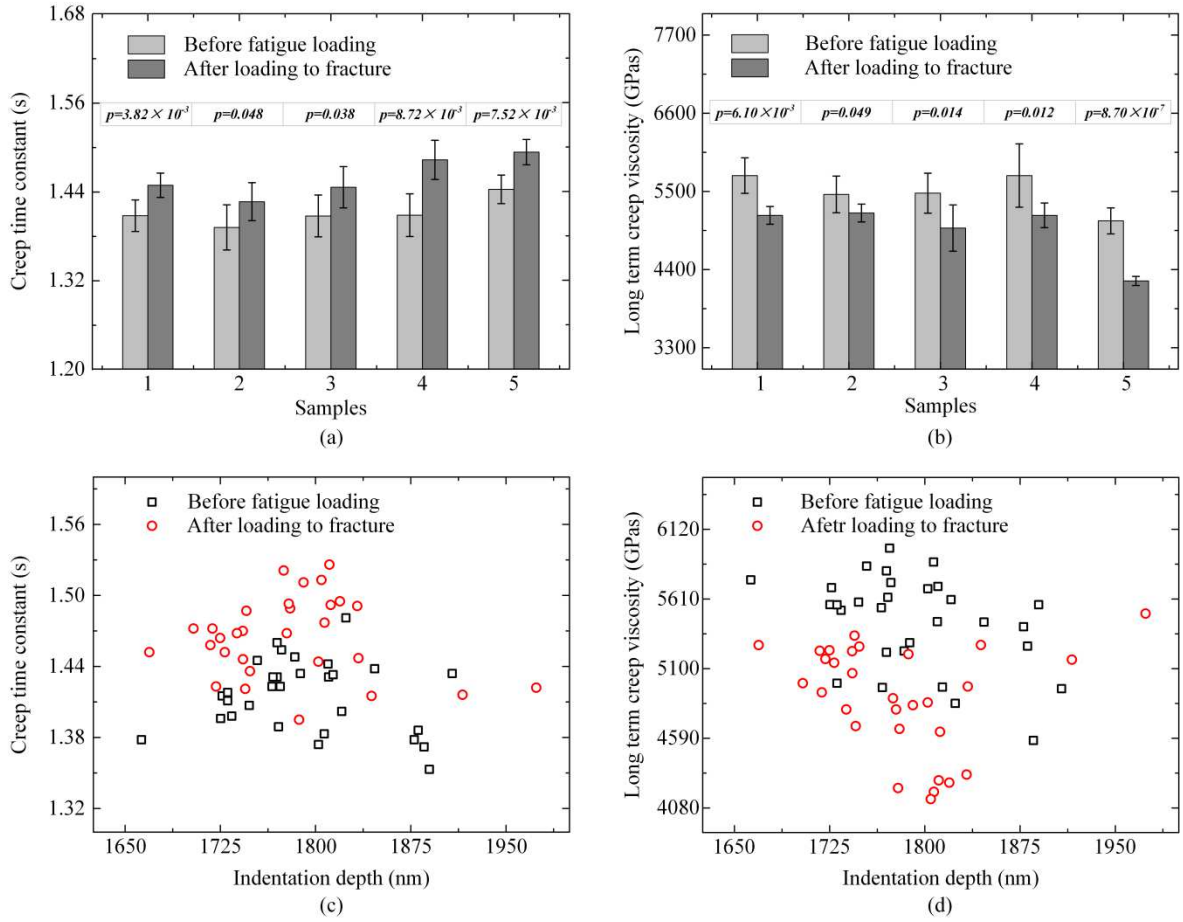

Fig. 5 - A graph of the parameters based on creep. (a) & (c) the creep time constants τ (s). (b) & (d) the long-term creep viscosity η (GPas).

A Burgers model captured bone's creep behavior. After fracture, the long-term creep viscosity changed from 5442±346 GPas to 4886±392 GPas while the time constant changed from 1.42±0.03 s to 1.46±0.03 s ($p<0.05$ for both). The variability of the creep parameters, quantified by the coefficient of variation (SD/mean), was larger for viscosity and lower for the time constants (Table 1). This is true both within and between samples.There was no obvious variation of the distribution of creep parameters with depth before fatigue loading and after loading to fracture.

3.4. Hardness and dissipated work (Figure 6)

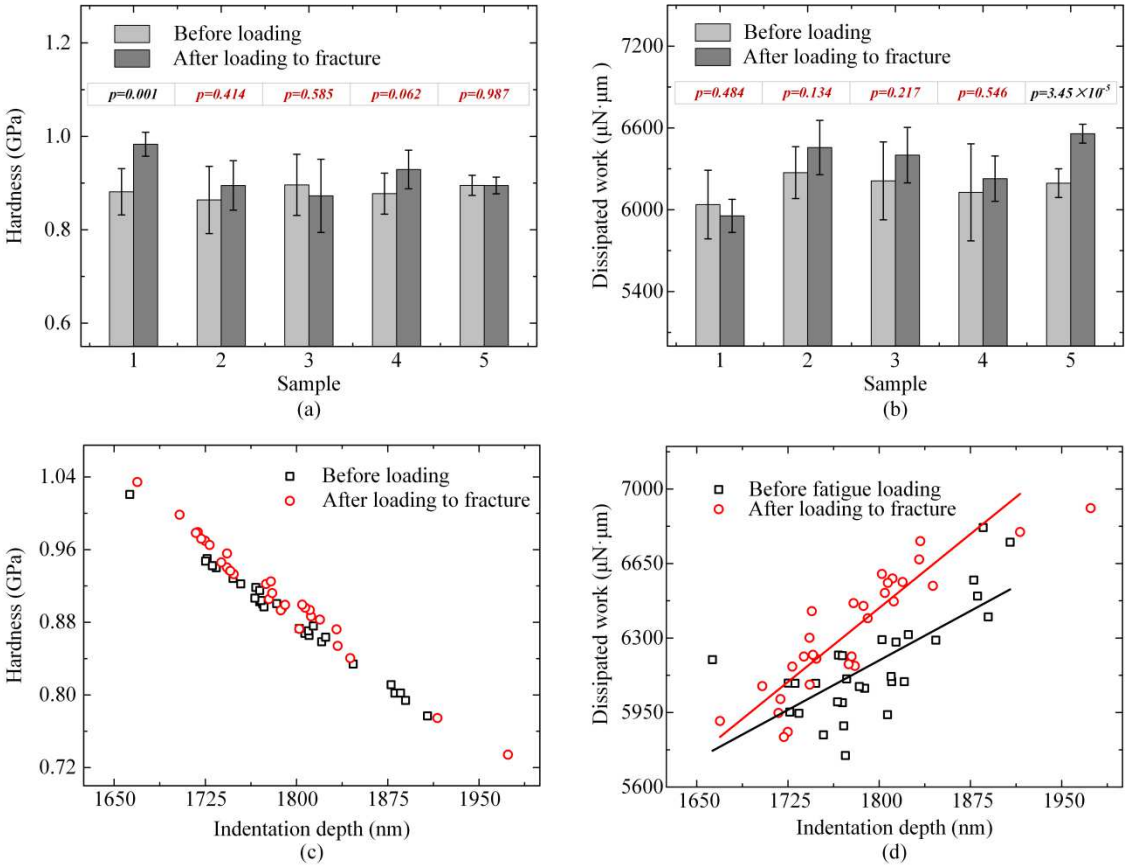

Fig. 6 - A graph of the hardness and dissipated work. (a) & (c) the hardness H (GPa). (b) & (d) the dissipated work (μN·μm). Before loading: D=3.10h+619, r^2=0.50; after loading to fracture: D=4.63h-1893, r^2=0.78, where D represents the dissipated work and h represents the indentation depth.

Before fatigue loading and after loading to fracture, the measured hardness was 0.883±0.051 GPa and 0.915±0.060 GPa respectively while the dissipated work was 6169±248 μN·μm and 6319±261 μN·μm respectively. Only the variation of hardness in sample 1 as well as that of dissipated work in sample 5 were significant. Despite fatigue loading, hardness values were always dependent on the indentation depth (Fig. 6c). After fracture, the slope that dissipated work varies with the indentation depth increased from 3.10 to 4.63 (Fig. 6d).

3.5. Normalized comparison

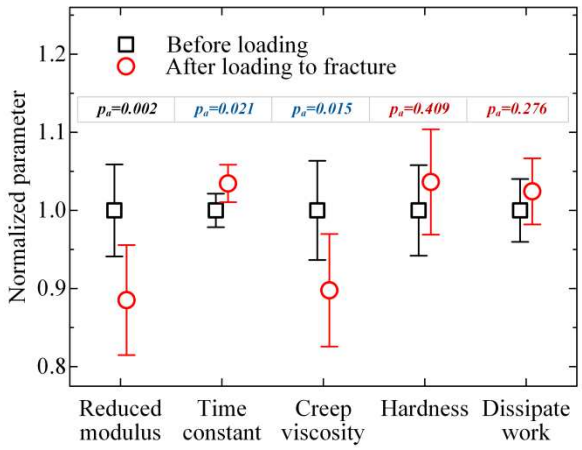

Fig. 7 - Comparison of the normalized parameters. Each parameter before loading was set to 1, the related parameter after loading to fracture was calculated proportionally.

As shown in Figure 7, the reduced modulus was more significantly different following fatigue loading than were the other parameters. The creep time constant increased and the long-term creep viscosity decreased (Pa=0.021 and 0.015, respectively) following fatigue loading. Although the average values for hardness and dissipated work increased slightly after fracture, Pa values did not reach statistical significance.

4. Discussion

The present study based on nanoindentation investigated the difference of bone's microscopic mechanical properties before fatigue loading and after loading to fracture. Reduced modulus, creep time constant and viscosity, hardness and dissipated work were calculated from the indentation curves. Paired t-tests were used to evaluate the differences caused by fatigue loading. The p-value was significantly lower ($p<0.001$) for reduced modulus compared to all other mechanical properties. As the material already was damaged by the first indentation, the indentation tests could create crack initiators that are unfavorable to fatigue strength. Using optical microscope and SEM, the initial residual indentation remained the same morphologically during the whole fatigue progress. The size of the indents was too small to create stress concentrations and they would have no effect on subsequent fatigue loading.

The values for hardness and reduced modulus are similar to the values reported in the literature[18, 43, 44]. As shown in Figure 6, the hardness also was dependent on indentation depth[45, 46]. Usually, modulus and hardness are approximately positively correlated. After fatigue loading, some lower modulus values were accompanied by greater hardness. Hardness varies by

sample (Fig. 6a), but the reduced modulus decreased in every case (Fig. 4a). Hardness ($H=P_{max}/A$) is only affected by the projected contact area at peak load A, while reduced modulus ($E_r = S \cdot \sqrt{\pi} / (2 \cdot \sqrt{A})$) is affected by both A and the measured stiffness S [13]. After fracture, S increased and A changed randomly. The obvious degradation of E_r indicates that the unloading slope S has the most significant effect on bone's reduced modulus under fatigue loading.

A Burgers model was used to calculate the mechanical properties based on creep, as this model is highly suitable to simulate the creep response of bone [25, 27]. Our creep time constants, agreeing with the results in human bone [47], were 30% lower than those from Berkovich indentation creep testing on bovine bone[27]. However, their specimens were wet and the hold time was 200 s which, along with the difference in indenter geometry, could be responsible for the difference. Long term viscosity is on the same order of magnitude as those of other studies [45]. Studies on bone have shown that the time constant using nanoindentation is an order of magnitude from the macroscopic results [45, 48], which is also confirmed by our results. Bone's hierarchical structure, the plastic and damage behavior from the indenters as well as loading and deformation conditions will all contribute to differences between microstructural and macroscopic properties.

The relationship between hardness and indentation depth was almost the same pre- and post-fatigue. There was no obvious variation in the distribution of creep parameters or reduced modulus with depth before fatigue loading and after loading to fracture. However, a slight variation was found in Figure 6d. The dissipated work was more related significantly influenced by indentation depth after loading to fracture, with the Pearson correlation coefficient increasing from 0.719 to 0.888. The increased slope indirectly indicates that plastic deformation related with dissipated work is more likely to occur in bone after fracture.

Reference samples were prepared to evaluate the method-dependent variations. The CV% value for hardness and modulus of perfectly smooth silica were more than one order of magnitude lower than that for the bone samples (Table 1). This suggests that the indentation instrument or setup is responsible for little of the variation in the bone measurements. The polished silica samples were prepared using the same protocol as the bone samples. The difference between the measurements for the polished and smooth silica can be attributed to the sample preparation protocol. In this study, this effects contributed to about 2% of the variation.

Table 1 - Coefficient of variation (CV%) for microscopic mechanical parameters of the reference materials and bone samples.

Samples	Modulus		Time constant		Creep viscosity		Hardness		Work	
	BL	AF	BL	AF	BL	AF	BL	AF	BL	AF
S1 (9.6)	2.62%	1.71%	1.54%	1.15%	4.36%	2.42%	5.62%	2.61%	4.17%	2.04%
S2 (5.5)	4.92%	3.74%	2.24%	1.83%	1.83%	4.73%	8.33%	5.92%	3.03%	3.09%
S3 (5.8)	3.39%	4.25%	2.04%	1.96%	5.14%	6.52%	7.32%	8.98%	4.60%	3.18%
S4 (3.4)	4.37%	3.22%	2.09%	1.82%	7.78%	3.35%	5.01%	4.45%	5.81%	2.67%
S5 (8.1)	2.54%	1.17%	1.36%	1.16%	3.60%	1.51%	2.41%	1.99%	1.70%	1.05%
All	5.89%	7.95%	3.03%	3.39%	6.35%	8.03%	5.12%	5.96%	4.02%	4.13%
Smooth	0.25%						0.52%		1.43%	
Polished	2.16%						3.43%		2.94%	

S=sample; BL=before loading; AF= after loading to fracture; All=all samples; Smooth=smooth silica; Polished=polished silica. The number in brackets represents the loading cycles (10^4).The creep parameters of silica were not considered in this study as its creep behavior (1nm/s) was affected by the thermal drift.

As shown in Table 1, the highly organized matrix in tibia and test area at microscopic level (30×120 um) in this study results in the small CV% values (Table 1) compared to other studies [43-45]. The trends of samples from the five different individual were consistent. Similar structures as well as the micro-area (30×120 um) also contributed to a stable data. Therefore, we conclude that the small sample size led to minor limitations. The bovine tibia in this study was dehydrated. Drying changes the mechanical properties but has no effect on the comparative trends between the samples or indentation location[49, 50]. Besides, dehydrated bone used in many studies contributed to controling the experimental environment [51].

5.Conclusions

From the nanoscale to the macroscopic scale, bone's hierarchical structure underlies its excellent mechanical properties [9, 52]. Microdamage is associated with bone remodeling[53-55]. However, micromechanical properties following fatigue damage determined using nano-indedntation is less covered in cortical bone. The primary strength of this study was the demonstration of the characterization of bone's microscopic mechanical properties by nanoindentation following fatigue loading. Residual indents different from fatigue damage created no crack initiators that would weaken bone's resistance to fatigue loading. Compared to hardness, dissipated work and parameters related to creep, the reduced modulus was most heavily affected by fatigue loading, which decreased by 7.62%~15.16% ($p=9.47\times10^{-3}$). Further studies are needed to investigate the exact mechanisms responsible for this. These founding are applicable to research on bone replacement materials, improve the field of clinical bone fractures, and provide an experimental reference for a more detailed model of bone fatigue damage.

Abbreviations:

SD: standard deviation; CV: Coefficient of variation; S: sample; BL: before loading; AF: after loading to fracture.

Declarations

Ethics approval and consent to participate

Cattle bones used in this study were taken from local slaughterhouses, and no animals were euthanized specifically for this study.

Consent for publication

Not applicable.

Data availability

The raw/processed data required to reproduce these findings cannot be shared at this time as the data also forms part of an ongoing study.

Competing Interest

There are no conflicts of interest to declare. The authors declare that they do not have any competing financial or associative interests that could influence the work submitted.

Funding: This work is financially supported by the National Natural Science Foundation of China (Grant Nos. 11972247 and 11772204).

Author Contributions

Xianjia Meng: Data curation, Formal analysis, Investigation, Validation, Writing-original draft. Qinghua Qin: Conceptualization, Supervision, Writing-review & editing. Chuanyong Qu: Methodology, Resources, Writing-original draft, Writing-review & editing, Supervision, Project administration, Funding acquisition.

Acknowledgments

The authors would like to express their gratitude to EditSprings (http://www.editsprings.com/) for the expert linguistic services provided.

Authors' information

1 Department of Mechanics, School of Mechanical Engineering, Tianjin University, Tianjin 300350, China

2 College of Engineering and Computer Science, Australian National University, Canberra, ACT 2601, Australia

Refernce

1. Currey JD: **Some effects of ageing in human Haversian systems.** *J Anat* 1964, **98**(Pt 1):69-75.

2. Jowsey J: **Studies of Haversian systems in man and some animals.** *J Anat* 1966, **100**(Pt 4):857-864.

3. Qin Q-H, Qu C, Ye J: **Thermoelectroelastic solutions for surface bone remodeling under axial and transverse loads.** *Biomaterials* 2005, **26**(33):6798-6810.

4. Qin QH: *Mechanics of Cellular Bone Remodeling: Coupled Thermal, Electrical, and Mechanical Field Effects.* CRC Press, Taylor & Francis, Boca Raton; 2013.

5. Tertuliano OA, Greer JR: **The nanocomposite nature of bone drives its strength and damage resistance.** *Nat Mater* 2016, **15**(11):1195-1202.

6. Wagermaier W, Klaushofer K, Fratzl P: **Fragility of Bone Material Controlled by Internal Interfaces.** *Calcif Tissue Int* 2015, **97**(3):201-212.

7. Fratzl P: **Biomimetic materials research: what can we really learn from nature's structural materials?** *J R Soc Interface* 2007, **4**(15):637-642.

8. Fratzl P, Gupta HS: **Nanoscale Mechanisms of Bone Deformation and Fracture.** In *Handbook of Biomineralization.* 2007: 397-414.

9. Fratzl P, Weinkamer R: **Nature's hierarchical materials.** *Prog Mater Sci* 2007, **52**(8):1263-1334.

10. Ritchie RO: **The conflicts between strength and toughness.** *Nat Mater* 2011, **10**(11):817-822.

11. Frost HL: **Presence Of Microscopic Cracks In Vivo In Bone.** *Henry Ford Hosp Med Bull* 1960, **8**(1):25-35.

12. Vashishth D, Koontz J, Qiu SJ, Lundin-Cannon D, Yeni YN, Schaffler MB, Fyhrie DP: **In vivo diffuse damage in human vertebral trabecular bone.** *Bone* 2000, **26**(2):147-152.

13. Oliver WC, Pharr GM: **An improved technique for determining hardness and elastic modulus using load and displacement sensing indentation experiments.** *J Mater Res* 1992, **7**(6):1564-1583.

14. Oliver WC, Pharr GM: **Measurement of hardness and elastic modulus by instrumented indentation: Advances in understanding and refinements to methodology.** *J Mater Res* 2004, **19**(1):3-20.

15. Zysset PK, Edward Guo X, Edward Hoffler C, Moore KE, Goldstein SA: **Elastic modulus and hardness of cortical and trabecular bone lamellae measured by nanoindentation in the human femur.** *J Biomech* 1999, **32**(10):1005-1012.

16. Feng L, Chittenden M, Schirer J, Dickinson M, Jasiuk I: **Mechanical properties of porcine femoral cortical bone measured by nanoindentation.** *J Biomech* 2012, **45**(10):1775-1782.

17. Faingold A, Cohen SR, Wagner HD: **Nanoindentation of osteonal bone lamellae.** *J Mech Behav Biomed Mater* 2012, **9**:198-206.

18. Tai K, Dao M, Suresh S, Palazoglu A, Ortiz C: **Nanoscale heterogeneity promotes energy dissipation in bone.** *Nat Mater* 2007, **6**(6):454-462.

19. Zhang J, Niebur GL, Ovaert TC: **Mechanical property determination of bone through nano- and micro-indentation testing and finite element simulation.** *J Biomech* 2008, **41**(2):267-275.

20. Zhang J, Michalenko MM, Kuhl E, Ovaert TC: **Characterization of indentation response and stiffness reduction of bone using a continuum damage model.** *J Mech Behav Biomed Mater* 2010, **3**(2):189-202.

21. McCalden RW, McGeough JA, Barker MB, Court-Brown CM: **Age-related changes in the tensile properties of cortical bone. The relative importance of changes in porosity, mineralization, and microstructure.** *J Bone Joint Surg Am* 1993, **75**(8):1193-1205.

22. Currey J: **Structural heterogeneity in bone: good or bad?** *J Musculoskelet Neuron Interact* 2005, **5**(4):317.

23. Burket J, Gourion-Arsiquaud S, Havill LM, Baker SP, Boskey AL, van der Meulen MCH: **Microstructure and nanomechanical properties in osteons relate to tissue and animal age.** *J Biomech* 2011, **44**(2):277-284.

24. Yin L, Venkatesan S, Webb D, Kalyanasundaram S, Qin Q-H: **Effect of cryo-induced microcracks on microindentation of hydrated cortical bone tissue.** *Mater Charact* 2009, **60**(8):783-791.

25. Fischer-Cripps AC: **A simple phenomenological approach to nanoindentation creep.** *Mater Sci Eng A* 2004, **385**(1):74-82.

26. Oyen ML: **Spherical Indentation Creep Following Ramp Loading.** *J Mater Res* 2005, **20**(8):2094-2100.

27. Wu Z, Baker TA, Ovaert TC, Niebur GL: **The effect of holding time on nanoindentation measurements of creep in bone.** *J Biomech* 2011, **44**(6):1066-1072.

28. Lakes RS, Katz JL, Sternstein SS: **Viscoelastic properties of wet cortical bone—I. Torsional and biaxial studies.** *J Biomech* 1979, **12**(9):657-678.

29. Les CM, Spence CA, Vance JL, Christopherson GT, Patel B, Turner AS, Divine GW, Fyhrie DP: **Determinants of ovine compact bone viscoelastic properties: effects of architecture, mineralization, and remodeling.** *Bone* 2004, **35**(3):729-738.

30. Les CM, Vance JL, Christopherson GT, Turner AS, Divine GW, Fyhrie DP: **Long-term ovariectomy decreases ovine compact bone viscoelasticity.** *J Orth Res* 2005, **23**(4):869-876.

31. Loundagin LL, Edwards WB: **Stressed volume around vascular canals explains compressive fatigue life variation of secondary osteonal bone but not plexiform bone.** *J Mech Behav Biomed Mater* 2020, **111**:104002.

32. Pattin CA, Caler WE, Carter DR: **Cyclic mechanical property degradation during fatigue loading of cortical bone.** *J Biomech* 1996, **29**(1):69-79.

33. Li S, Abdel-Wahab A, Silberschmidt VV: **Analysis of fracture processes in cortical bone tissue.** *Eng Fract Mech* 2013, **110**:448-458.

34. Subit D, Dios EdPd, Valazquez-Ameijide J, Arregui-Dalmases C, Crandall J: **Tensile material properties of human rib cortical bone under quasi-static and dynamic failure loading and influence of the bone microstucture on failure characteristics.** *Physics* 2011.

35. Trębacz H, Zdunek A, Cybulska J, Pieczywek P: **Effects of fatigue on microstructure and mechanical properties of bone organic matrix under compression.** *Australas Phys Eng Sci Med* 2013, **36**(1):43-54.

36. Locke M: **Structure of long bones in mammals.** *J Morphol* 2004, **262**(2):546-565.

37. Sasso M, Haïat G, Yamato Y, Naili S, Matsukawa M: **Dependence of ultrasonic attenuation on bone mass and microstructure in bovine cortical bone.** *J Biomech* 2008, **41**(2):347-355.

38. Erben RG: **Embedding of Bone Samples in Methylmethacrylate: An Improved Method Suitable for Bone Histomorphometry, Histochemistry, and Immunohistochemistry.** *J Histochem Cytochem* 1997, **45**(2):307-313.

39. Rho J-Y, Tsui TY, Pharr GM: **Elastic properties of human cortical and trabecular lamellar bone measured by nanoindentation.** *Biomaterials* 1997, **18**(20):1325-1330.

40. Donnelly E, Baker SP, Boskey AL, van der Meulen MCH: **Effects of surface roughness and maximum load on the mechanical properties of cancellous bone measured by nanoindentation.** *J Biomed Mater Res A* 2006, **77A**(2):426-435.

41. Draper ERC, Goodship AE: **A novel technique for four-point bending of small bone samples with semi-automatic analysis.** *J Biomech* 2003, **36**(10):1497-1502.

42. Hengsberger S, Ammann P, Legros B, Rizzoli R, Zysset P: **Intrinsic bone tissue properties in adult rat vertebrae: modulation by dietary protein.** *Bone* 2005, **36**(1):134-141.

43. Norman J, Shapter JG, Short K, Smith LJ, Fazzalari NL: **Micromechanical properties of human trabecular bone: A hierarchical investigation using nanoindentation.** *J Biomed Mater Res A* 2008, **87A**(1):196-202.

44. Fan Z, Rho J-Y: **Effects of viscoelasticity and time-dependent plasticity on nanoindentation measurements of human cortical bone.** *J Biomed Mater Res A* 2003, **67A**(1):208-214.

45. Isaksson H, Nagao S, MałŁkiewicz M, Julkunen P, Nowak R, Jurvelin JS: **Precision of nanoindentation protocols for measurement of viscoelasticity in cortical and trabecular bone.** *J Biomech* 2010, **43**(12):2410-2417.

46. Chaudhry B, Ashton H, Muhamed A, Yost M, Bull S, Frankel D: **Nanoscale viscoelastic properties of an aligned collagen scaffold.** *J Mater Sci Mater Med* 2009, **20**(1):257.

47. Wu Z, Ovaert TC, Niebur GL: **Viscoelastic properties of human cortical bone tissue depend on gender and elastic modulus.** *J Orth Res* 2012, **30**(5):693-699.

48. Iyo T, Maki Y, Sasaki N, Nakata M: **Anisotropic viscoelastic properties of cortical bone.** *J Biomech* 2004, **37**(9):1433-1437.

49. Rho J-Y, Pharr GM: **Effects of drying on the mechanical properties of bovine femur measured by nanoindentation.** *J Mater Sci Mater Med* 1999, **10**(8):485-488.

50. Hengsberger S, Kulik A, Zysset P: **Nanoindentation discriminates the elastic properties of individual human bone lamellae under dry and physiological conditions.** *Bone* 2002, **30**(1):178-184.

51. Lewis G, Nyman JS: **The use of nanoindentation for characterizing the properties of mineralized hard tissues: State-of-the art review.** *J Biomed Mater Res B Appl Biomater* 2008, **87B**(1):286-301.

52. Qin Q-H, Ye J-Q: **Thermoelectroelastic solutions for internal bone remodeling under axial and transverse loads.** *Int J Solids Struct* 2004, **41**(9):2447-2460.

53. Qu C, Qin Q-H, Kang Y: **A hypothetical mechanism of bone remodeling and modeling under electromagnetic loads.** *Biomaterials* 2006, **27**(21):4050-4057.

54. Bentolila V, Boyce TM, Fyhrie DP, Drumb R, Skerry TM, Schaffler MB: **Intracortical remodeling in adult rat long bones after fatigue loading.** *Bone* 1998, **23**(3):275-281.

55. Burr DB, Martin RB, Schaffler MB, Radin EL: **Bone remodeling in response to in vivo fatigue microdamage.** *J Biomech* 1985, **18**(3):189-200.

Figures

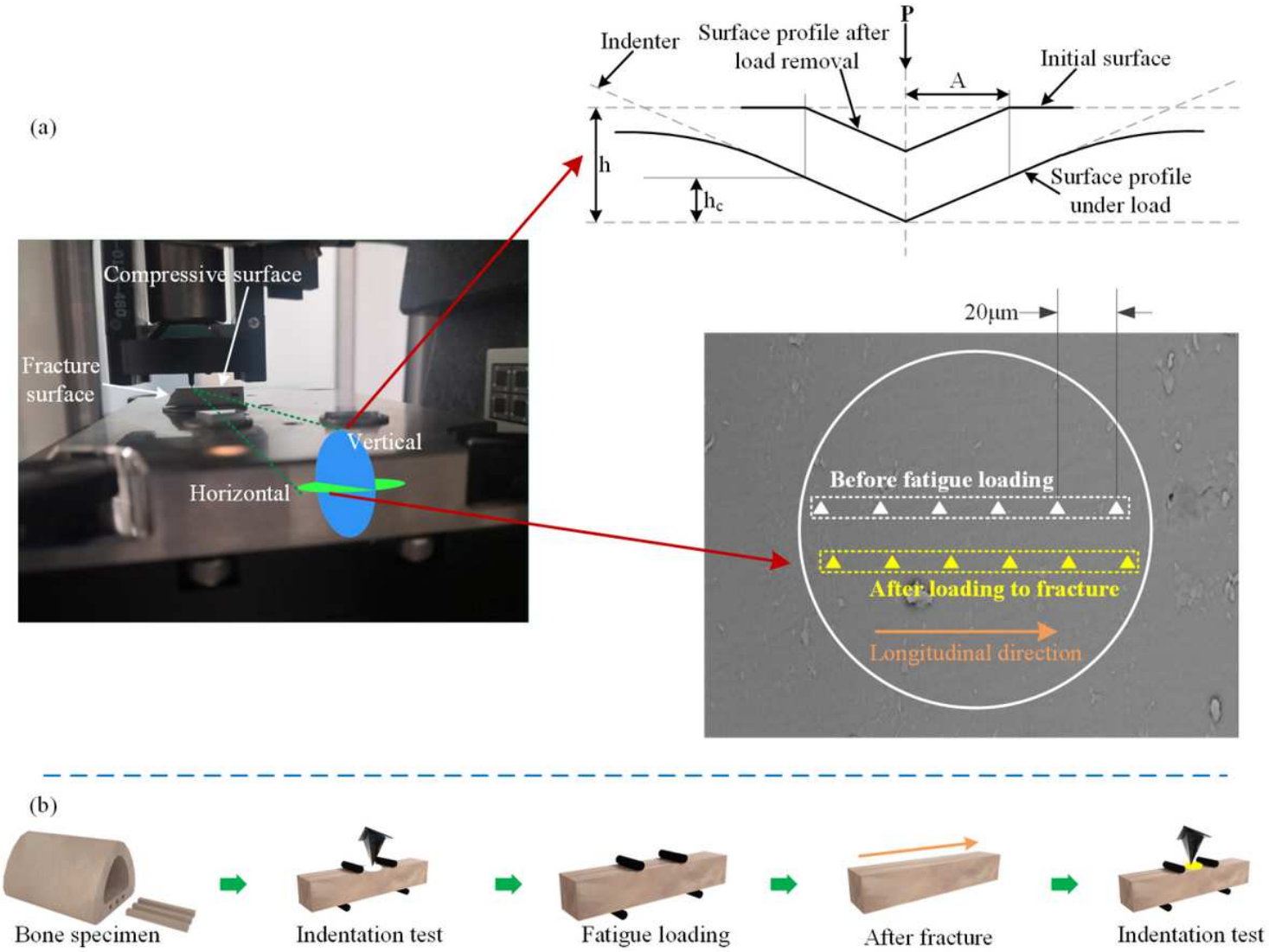

Figure 1

A graphic of the indentation test. (a) Bone samples were affixed to the measuring gasket using double-sided adhesive tape. (b) According to the Oliver and Pharr method, the area of contact at peak load is determined by the geometry of the indenter and the depth of contact, A=F(hc). (c) To avoid mutual influence between indentations, the spacing of each indentation should be at least 5 times greater than the indentation depth. The setting in this study (more than 12 times) meets this requirement.

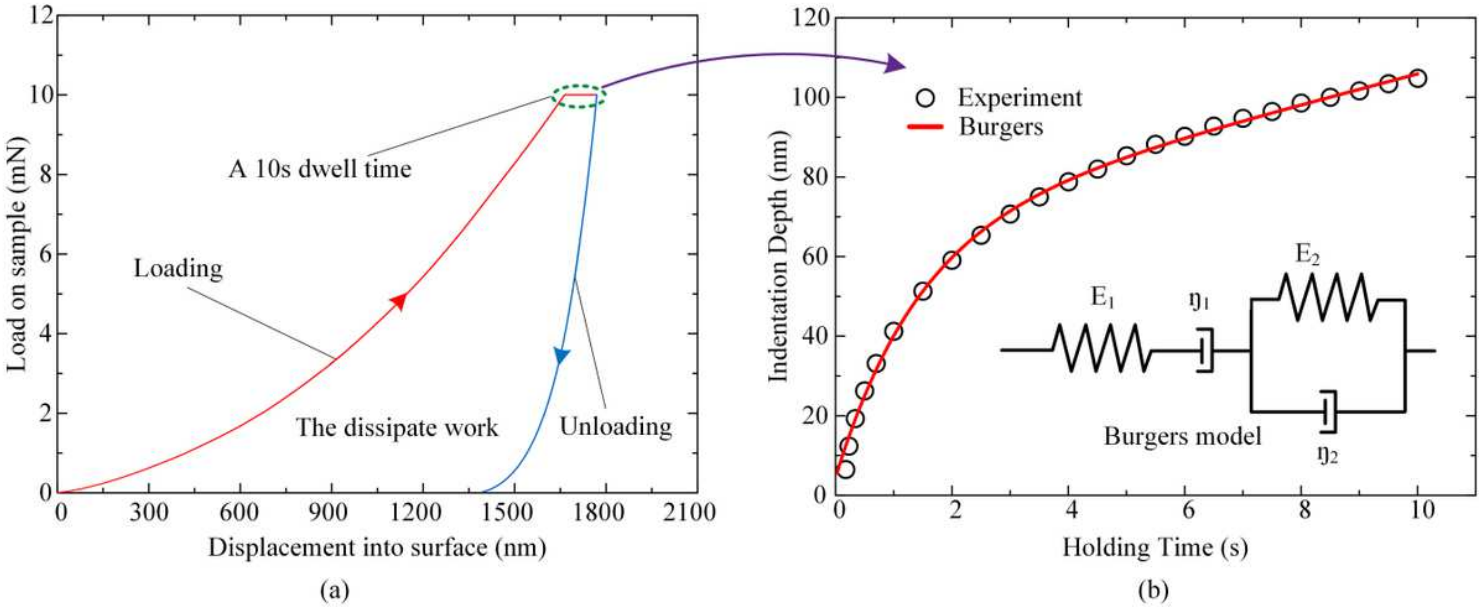

Figure 2

A graphic of the load-displacement curves and creep data. (a) The area bound by the load-displacement curve is dissipated work. (b) A representative creep data set and curve fits for the Burgers model with two elastic and two viscous elements. The time constant is theoretically given by E2/η2.

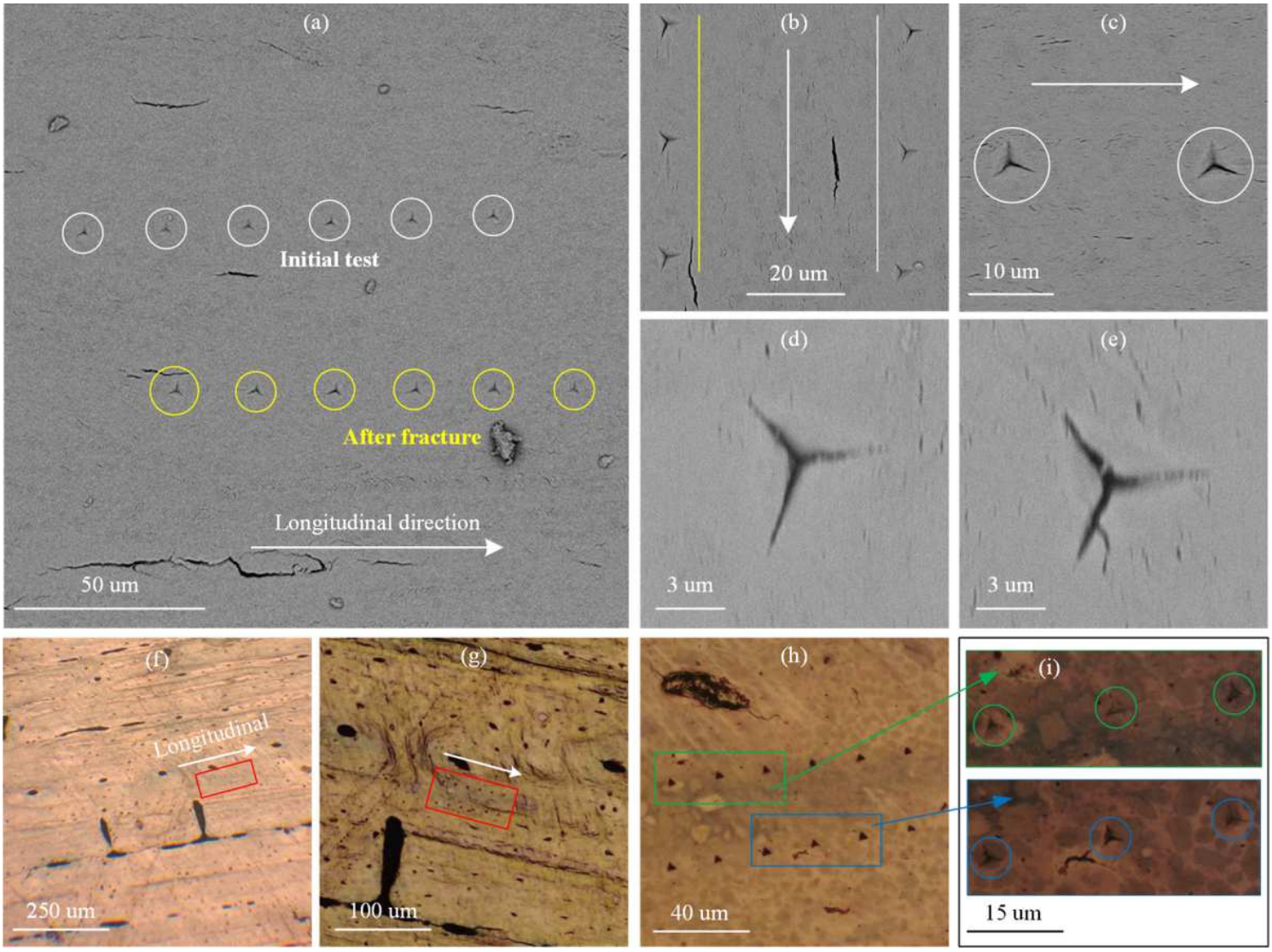

Figure 3

A graphic of the residual indentations. (a) & (b) the residual indentations before fatigue loading and after loading to fracture. (c), (d) & (e) the residual indentation morphology left by the initial test after loading to fracture. (f) (g) (h) (i) Optical microscope images. The red is the residual indentations from the two tests. The green is the initial test and the blue is the second test.

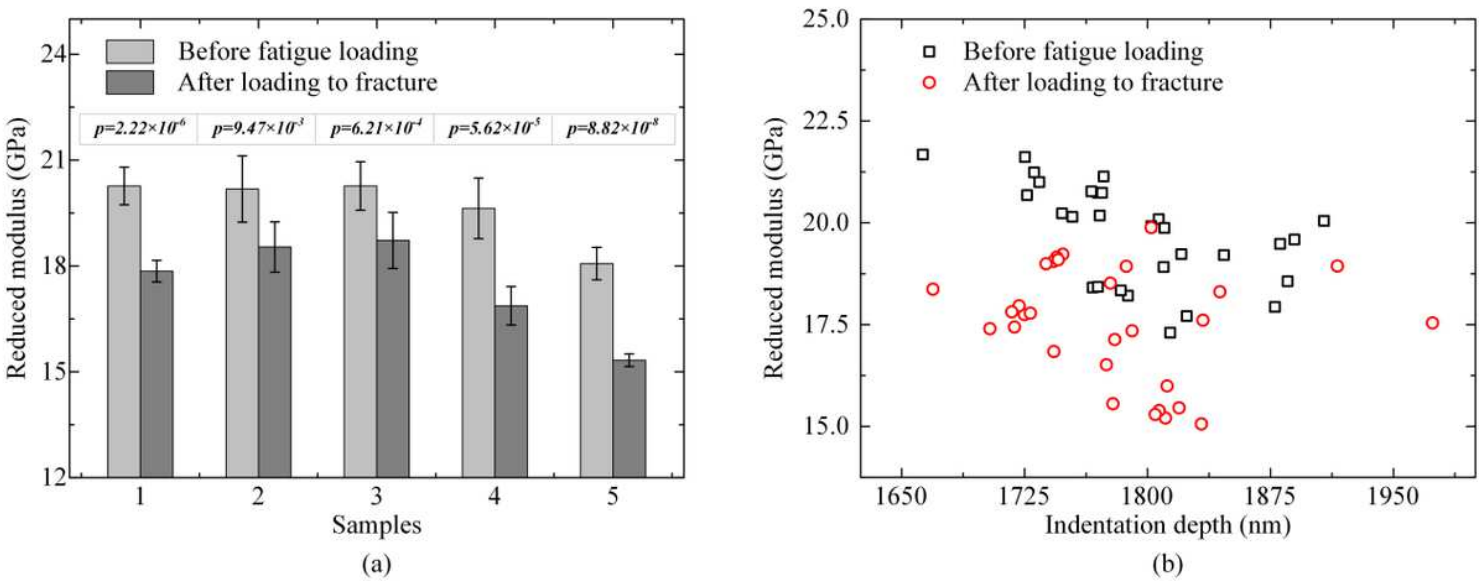

Figure 4

A graph of the reduced modulus. (a) The reduced modulus of each sample. (b) The reduced modulus of all samples.

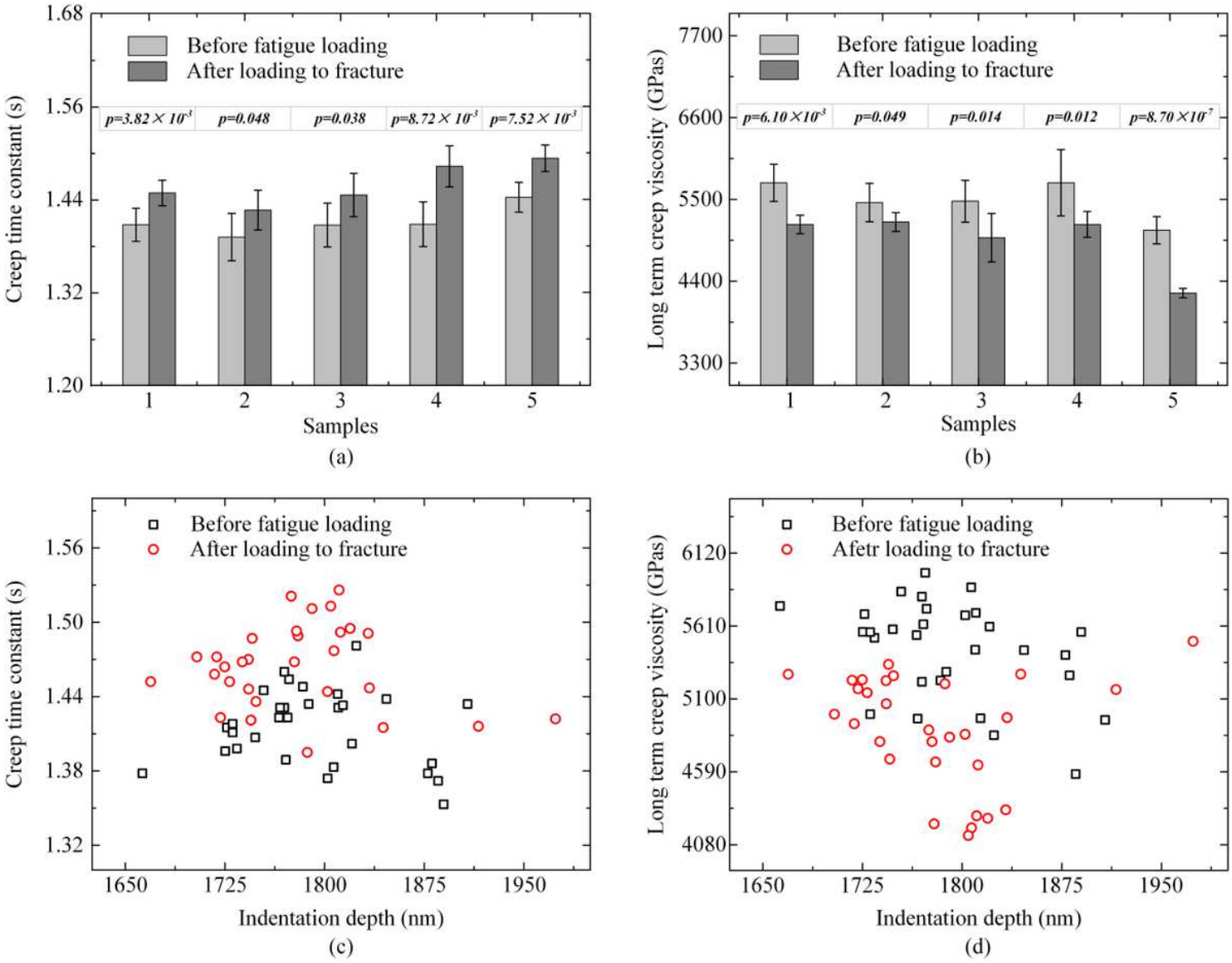

Figure 5

A graph of the parameters based on creep. (a) & (c) the creep time constants τ (s). (b) & (d) the long-term creep viscosity η (GPas).

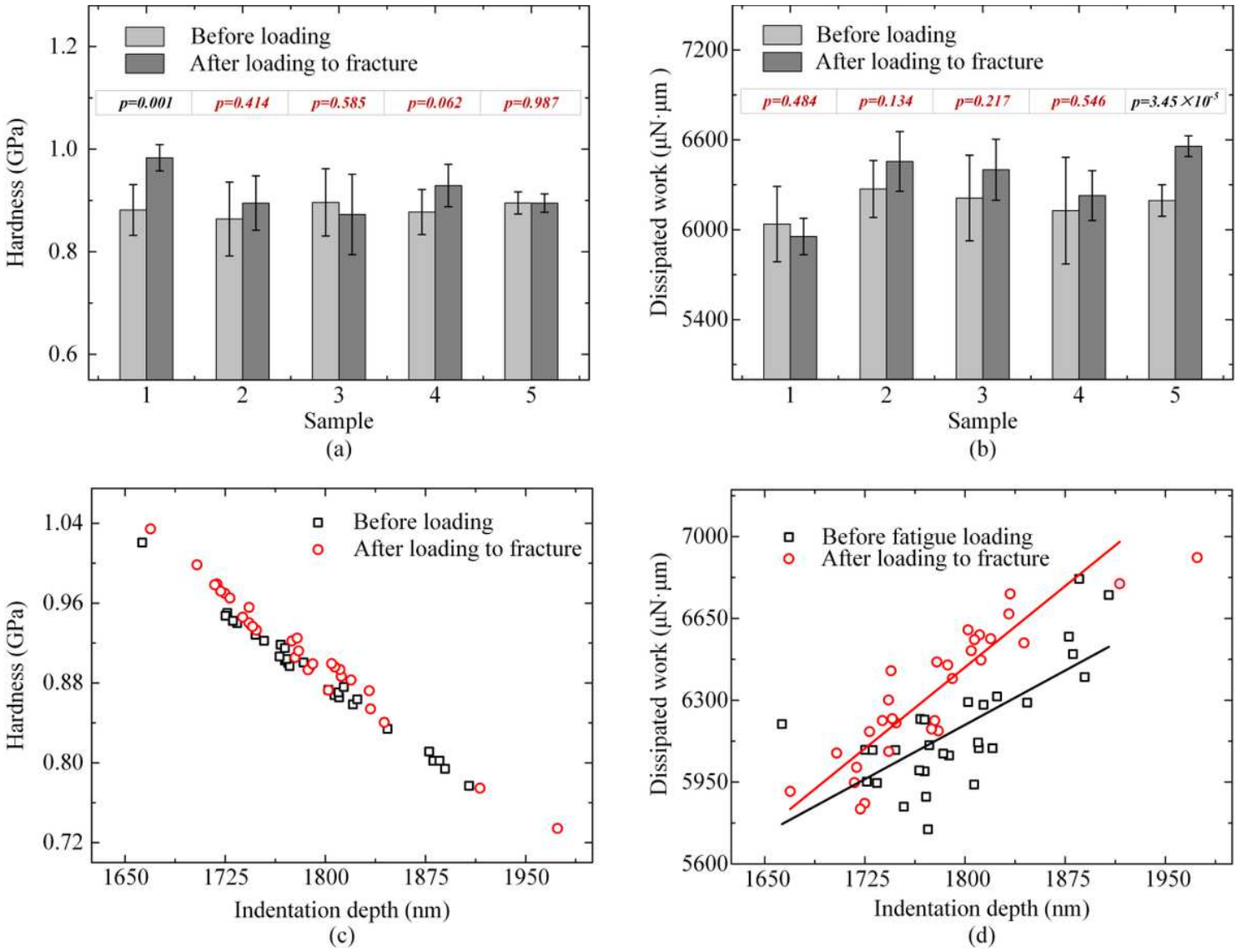

Figure 6

A graph of the hardness and dissipated work. (a) & (c) the hardness H (GPa). (b) & (d) the dissipated work (μN·μm). Before loading: D=3.10h+619, r2=0.50; after loading to fracture: D=4.63h-1893, r2=0.78, where D represents the dissipated work and h represents the indentation depth.

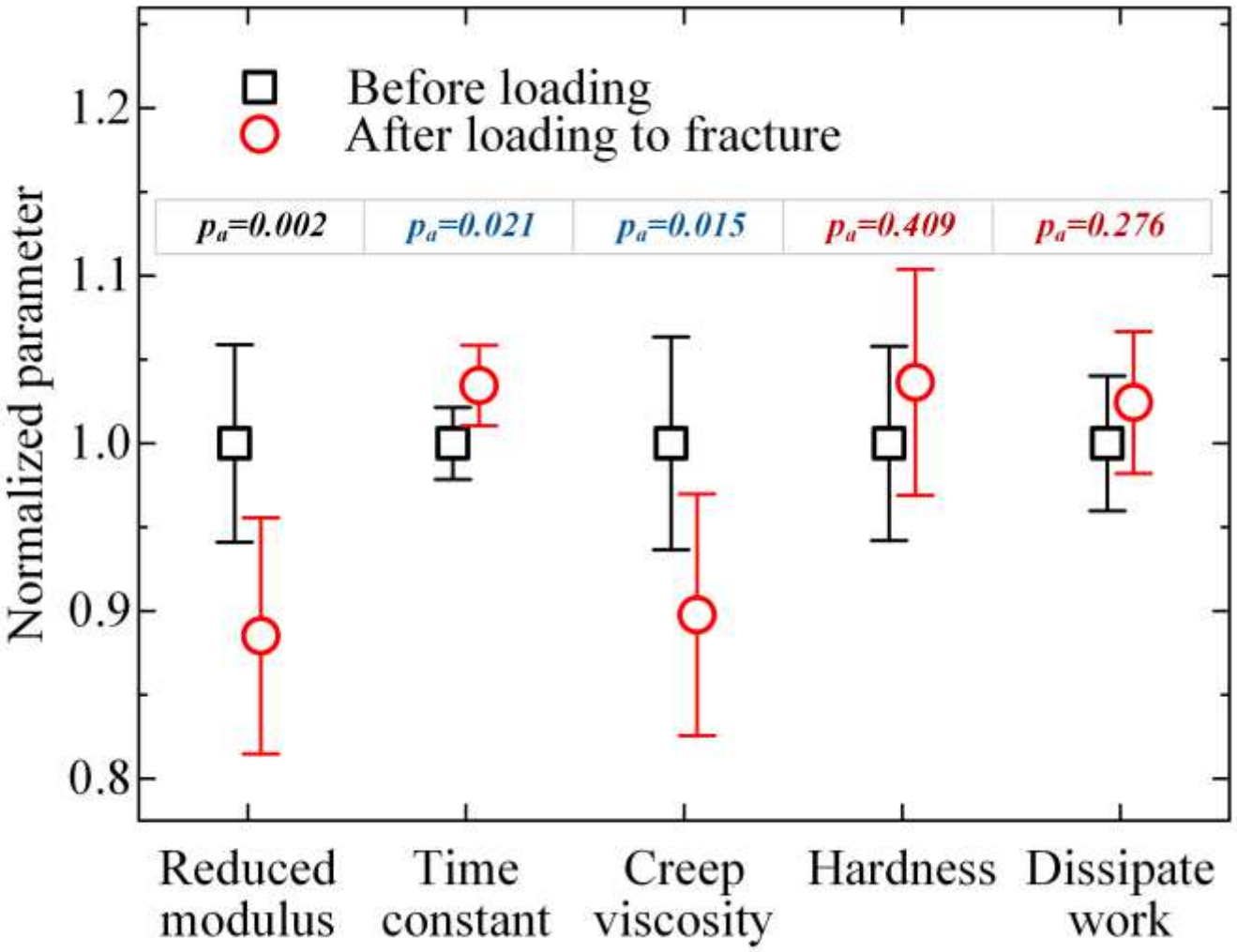

Figure 7

Comparison of the normalized parameters. Each parameter before loading was set to 1, the related parameter after loading to fracture was calculated proportionally.